Postprint of: Alfuth J., Czapik A., Zadykowicz B., Olszewska T., Hydrogen and chalcogen bonds in crystals of chalcogenadiazolecarboxylic acids – competition or cooperation?, CRYSTENGCOMM, Vol. 26, iss. 22 (2024), pp. 2918-2927, DOI: 10.1039/D4CE00273C

Hydrogen and Chalcogen Bonds in Crystals of Chalcogenadiazolecarboxylic Acids – Competition or Cooperation?

Jan Alfuth, [a,*] Agnieszka Czapik, [b] Beata Zadykowicz, [c] Teresa Olszewska [a]

[a] *Department of Organic Chemistry, Faculty of Chemistry, Gdańsk University of Technology, 80-233 Gdańsk, Poland*
[b] *Department of Organic Stereochemistry, Faculty of Chemistry, Adam Mickiewicz University in Poznań, Poznań 61-614, Poland*
[c] *Laboratory of Luminescence Research, Faculty of Chemistry, University of Gdańsk, 80-308 Gdańsk, Poland*

Abstract

This article presents crystal structures of chalcogenadiazolecarboxylic acids bearing both a hydrogen and a chalcogen bond donor. The selected molecules varied in the size of the aromatic unit, the chalcogen atom and/or the position of the carboxyl group in the core structure. The most common synthons in their lattice are $R_2(8)$ self-complementary acid dimers or four-membered $[Ch\cdots N]_2$ rings. Supramolecular synthons where chalcogenadiazole moieties interact with the carboxyl group were also identified. Both ESP calculations and experimental data showed that all the studied molecules adopted flat conformations, but only in the case of three crystal structures were flat sheets observed. To assess the contribution of hydrogen and chalcogen bonds to the stabilization of the crystal structure, crystal lattice energy calculations were performed.

Introduction

One of the main challenges of crystal engineering is the ability to control the crystal structure of a one- or multi-component solid.[1] This is crucial in the design and synthesis of functional materials with the desired physico-chemical properties (optical, magnetic, thermal *etc*.). Hydrogen bonds (HBs) and σ-hole interactions (where a Lewis base interacts with the electron-depleted region of a covalently-bonded atom) are the basic tools used in crystal engineering. The latter are an attractive alternative to hydrogen bonds, predominantly due to their higher directionality – a very important aspect in crystal structure prediction. Over the last two decades, there have been multiple reports on the characteristics and applications of the above mentioned interactions, especially halogen bonds (XBs)[2,3] and chalcogen bonds (ChBs).[4,5] Very recently new bonds, formed by elements of the d-block of the periodic table, have been identified and given names such as the matere bond (MaB)[6] and the osme bond (OsB).[7] So far, the majority of supramolecular functional materials have been stabilized by hydrogen and π-stacking interactions.[8,9] Now however, new materials are often more complex and utilize other noncovalent bonds.[10,11]

Designing and/or predicting the architecture of a solid based on the molecular structure of the starting compound(s) can be challenging, even more so when the molecule has two or three functional groups that are chemically different, but form interactions of similar nature and energy. Hence, the need to study the competition (or cooperation) between these bonds during the transition of molecules from a solution to a crystal. In the literature, there are several reports regarding this topic. They mainly focus on the most well-known interactions, including the investigation of HB *vs.* XB,[12–19] HB *vs.* XB *vs.* π-π,[20] XB *vs.* ChB,[21–24] and some others.[25–27] The competition between ChBs and other interactions is much less studied and only a few articles have been published to date. For instance, competition and balance between intramolecular HBs and chalcogen-chalcogen interactions were investigated in *β*-chalcogenovinylaldehydes[28] and peri-substituted naphthalenes.[29] Recently, Scheiner demonstrated the possibility of tuning the strength of hydrogen and chalcogen bonds in a cyclic heterosynthon formed by a carboxylic acid and a 1,2,5-chalcogenadiazole ring using appropriate electron-withdrawing or donating substituents in the two components of this synthon.[30] It should be noted that the articles mentioned above presented purely theoretical approach. Experiential work that nicely presented the preferences in formation of intermolecular HBs and ChBs was done by Wang *et al.*[31] The authors obtained 1:1 and 2:1 cocrystals of isophthalic acid and 2,1,3-benzoselenadiazole and confirmed the coexistence of both seven

membered [COOH]–[Se···N] heterosynthon as well as acid–acid homosynthon in the crystal structure of the second cocrystal.

To the best of our knowledge, no experimental research has been published to date which would be focused on the structure-directing competition between hydrogen and chalcogen bonds in the crystal structures of compounds where HB and ChB donors and acceptors are incorporated in the same backbone. For this reason, we designed a series of simple model compounds – 1,2,5-chalcogenadiazole derivatives (**1**–**3**, Fig. 1) – popular building blocks used, for instance in crystal engineering,[32–34] optoelectronics,[35,36] luminescent materials,[37,38] anion recognition,[39] and polymers.[40,41]

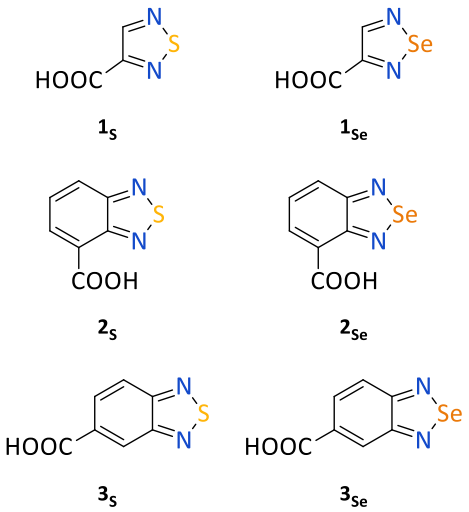

Fig. 1 Molecular structures of chalcogenadiazolecarboxylic acids **1**–**3** studied in this paper.

The heterocycles contain a carboxyl group and an S or an Se atom, thus all the molecules possess both a strong HB and a ChB donor. At the same time, the heterocyclic N atoms are good acceptors of both of these interactions. There are three variables in the series: the size of the rigid aromatic part of the molecule, the chalcogen atom with different ChB donor abilities, and the position of the COOH group. These features should provide the answer to the hierarchy of hydrogen and chalcogen bonds in the solid state. They should also provide insight as to whether strong HBs interfere with the formation of the $[Se\cdots N]_2$ supramolecular synthon (observed for many 1,2,5-selenadiazole derivatives[42]) and *vice versa* – whether strong ChBs interfere with the formation of the acid–acid synthon.

Experimental

Synthesis

1,2,5-Thiadiazole-3-carboxylic acid (**1S**) was prepared starting from acid hydrolysis of 1,2,5-thiadiazole-3,4-dicarbonitrile to obtain 1,2,5-thiadiazole-3,4-dicarboxylic acid, which was then thermally decarboxylated (Fig. 2). Unfortunately, the selenium derivative (**1Se**) could not be obtained *via* this procedure, nor *via* any other methods tried, including the direct reaction of 2,3-diaminopropionic acid with SeO_2.

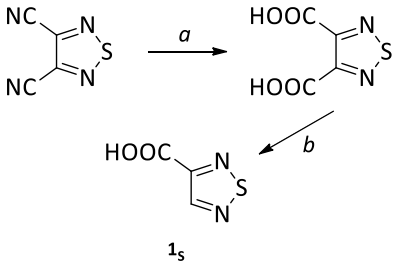

Fig. 2 Synthetic route for obtaining $\mathbf{1_S}$: (*a*) 6M HCl_{aq}, reflux, overnight; (*b*) 200°C, vacuum, 5 min.

2,1,3-Benzochalcogenadiazolecarboxylic acids **2**–**3** were synthesised according to the route shown in Fig. 3. First, methyl diaminobenzoates were obtained (instead of a direct reaction of the diamines with $SOCl_2$) to avoid the formation of acyl chlorides and to facilitate the purification process of the final products. Then, a heterocycle was formed leading to methyl 2,1,3-benzochalcogenadiazolecarboxylates (**4**–**5**) and lastly, alkaline hydrolysis and acidification yielded the desired acids (**2**–**3**). The experimental details, characterisation of the products and information on the crystallisation methods are presented in ESI.

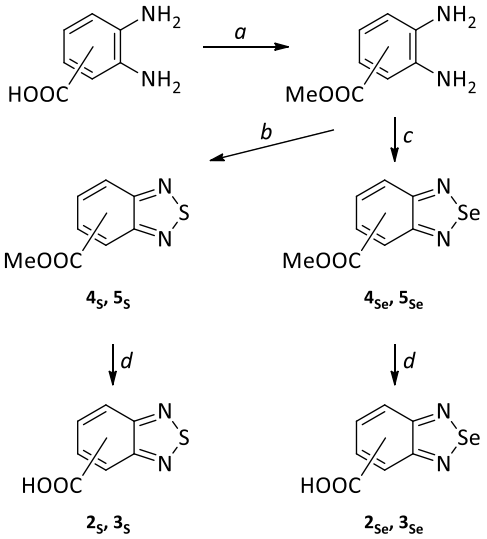

Fig. 3 Synthetic route for obtaining 2,1,3-benzochalcogenadiazolecarboxylic acids **2**–**3**: (*a*) $SOCl_2$, MeOH, 0°C then 45°C, overnight, (*b*) $SOCl_2$, Et_3N, DCM, 0°C then reflux, overnight, (*c*) SeO_2, anhydrous MeOH, reflux, 5 min, (*d*) 1M $NaOH_{aq}$, dioxane, RT, overnight, then 1M HCl_{aq}.

Crystal structure determination and refinement

Single crystals suitable for X-ray structural analysis were obtained by the slow evaporation of the chosen solvent (detailed information is given in ESI). The diffraction data for most of the compounds were collected at 130 K with an Oxford Diffraction SuperNova diffractometer using Cu Kα radiation (λ = 1.54184 Å) equipped with a mirror monochromator, whereas the diffraction data for $\mathbf{2_S}$ and $\mathbf{2_{Se}}$ were collected at 100K with an Oxford Diffraction Xcalibur diffractometer using Mo Kα radiation (λ = 0.71073 Å) graphite monochromator. The intensity data were collected and processed using CrysAlis PRO software.[43] The structures were solved by direct methods with the SHELXT 2018/2 program[44] and refined by the full-matrix least-squares method on F^2 with SHELXL 2018/3.[45] The carbon-bound hydrogen atoms were refined as riding on their carriers and their displacement parameters were set at 1.2Ueq(C). The hydrogen atoms of OH groups were located on electron-density difference maps. In the final cycles of the refinement, they were included in the calculated position and treated as riding atoms.

The crystals of $\mathbf{3_S}$ and $\mathbf{5_{Se}}$ were twinned and this was taken into account in the data reduction process. The refined BASF factor was 0.4135(14) for the $\mathbf{3_S}$ crystal, and 0.1171(11) for the $\mathbf{5_{Se}}$ crystal. Mercury[46] was used to prepare Figures 7–10. The crystallographic data and selected details of the structural refinement are summarized in Table S2 in ESI. Geometric parameters of the selected hydrogen and chalcogen bonds are juxtaposed in Table 1.

CCDC 2332628-2332636 contain supplementary crystallographic data. These data can be obtained free of charge *via* www.ccdc.cam.ac.uk/data_request/cif, by emailing data_request@ccdc.cam.ac.uk, or by contacting The Cambridge Crystallographic Data Centre, 12 Union Road, Cambridge CB2 1EZ, UK; fax: +44 1223 336033.

Theoretical calculations

Molecular electrostatic potential (MEP) maps

The geometry of molecules **1**–**3**, as well as of 2,1,3-benzothiadiazole and 2,1,3-benzoselenadiazole, was optimized in the gas phase (vacuum) at the B3LYP/6-31G**[47–51] level of theory using Gaussian16 package.[52] Frequency calculations were included in order to check whether true energy minima were achieved and no negative frequency values were obtained. Conformational analysis was performed in order to obtain the structure with the lowest energy. Two local minima were found for each of the compounds: with the carbonyl oxygen atom either closest to (conformer *syn*) or farthest from the heterocyclic nitrogen atom (conformer *anti*) (an example is shown in Fig. 4). The *anti* conformers displayed slightly lower energy values (see Figure S1 in ESI) and molecular electrostatic potential maps were generated based on those conformations. The ESP maps were calculated and visualized with GaussView 6.1.1.[53]

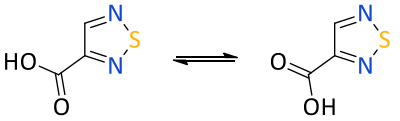

***syn*-1$_S$** ***anti*-1$_S$**

Fig. 4 Molecular structures of the *syn* and *anti* conformations of **1$_S$**.

Intermolecular interaction energies

Intermolecular interaction energies were calculated using Gaussian16 package[52] at the B3LYP/6-31++G**[47–49,54,55] or B3LYP/6-31G**[47–51] level of theory for sulphur or selenium derivatives respectively, with frequency calculations to confirm that no negative frequency values were obtained. The interaction energy (ΔE_{int}) was calculated as the difference between the energy of optimized dimer (E_{dimer}) and the combined energy of two optimized individual molecules of chalcogenadiazolecarboxylic acid ($E_{monomer}$) according to the equation: $\Delta E_{int} = E_{dimer} - 2E_{monomer}$. The obtained energies were corrected for the basis set superposition error (BSSE) by using the counterpoise method.[56] Only the centrosymmetric version of synthon **A** was used. For synthon **B**, three relative arrangements of molecules were implemented into the calculations. The results are presented in Table 2 and Table S1 in ESI.

Crystal lattice energies

The calculations were carried out with the periodic *ab initio* CRYSTAL17 program[57] at the DFT[58] level of theory using M06-2X[59] functional together with the 6-31G(d,p)[50,51] basis set with the DFT-D3 dispersion correction[60,61] to describe weak van der Waals-type dispersion interactions in the investigated compound. For a given experimental crystal structure, single point calculations of the periodic wave function and energy were performed. The total energies, calculated as the sum of electronic energy and nuclear repulsion energy, were used to compute the cohesive energy of the crystal:[62]

$$E_c = \frac{E_{bulk}}{Z} - E_{mol}$$

where E_{bulk} is the total energy of the unit cell, Z is the number of molecules in the unit cell, and E_{mol} is the total energy of the molecule extracted from the bulk. The *ab initio* DFT total energy values obtained at the M06-2X level of theory were subsequently corrected to take into account dispersive interactions. We employed damped empirical potential $-f(R)C_6/R^6$ (originally proposed by Grimme[60,61] and more recently calibrated by Civalleri *et al.*[62]) to improve the reliability of dispersion energy predictions for molecular crystals treated at the M06-2X level of theory. In this expression, R denotes interatomic distances and $f(R)$ is the damping function which preserves double counting of the energies of the short-range interactions already accounted for by a DFT calculation. The atomic coefficients C_6 were taken from ref. [53]. In order to avoid overestimation of the strength of interactions

within the crystals, cohesive energies E_c were additionally corrected for the basis set superposition error by the counterpoise method[56] implemented in the CRYSTAL17 code. Some ghost atoms used for BSSE estimation were selected up to 5 Å from the central molecule.[62]

Results and discussion

Electrostatic potential (ESP) maps

It has become a standard practise to precede the empirical study with theoretical calculations of electrostatic potential (ESP) maps of molecules so as to confirm the presence of regions most prone to form secondary bonding interactions (as donors as well as acceptors).[63] The ESP calculations identified the expected areas of high electrostatic potential for the compounds in this paper: one on the hydrogen atom of the COOH and two on the S and Se atoms corresponding to their two σ-holes (Fig. 5).

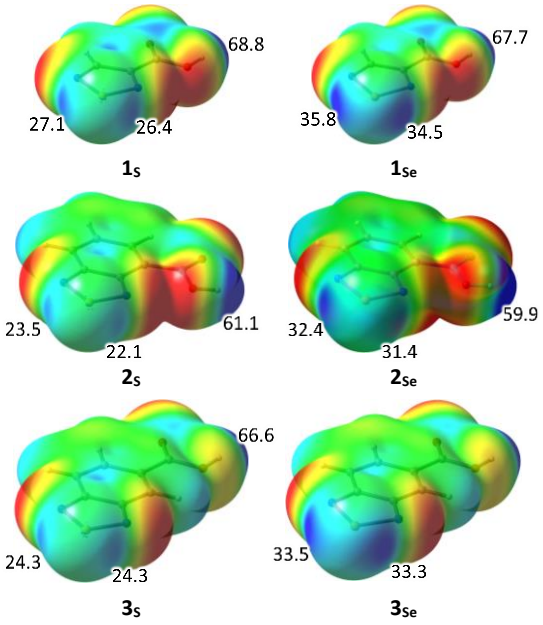

Fig. 5 Molecular electrostatic potential maps of chalcogenadiazolecarboxylic acids **1**–**3** mapped on 0.002 au electron density isosurface. The colour scale corresponds to values ranging from −0.04 (red) to +0.05 au (blue). The most positive ESP values for carboxylic hydrogen atoms and the two σ-holes of S or Se are indicated (in kcal/mol).

In each case, the carboxylic hydrogen atom has the highest ESP value, *ca.* 60–70 kcal/mol, which makes it twice as high as that of the Se σ-holes and tree times as high as that of the of the S σ-holes. Due to the dissymmetry of the molecules the electron density is not distributed evenly, but there is only a minimal difference between the two σ-holes of the S and Se atoms. On the other hand, the ESP differences observed for **1**$_S$, **1**$_{Se}$, **2**$_S$ and **2**$_{Se}$ are greater than those for **3**$_S$ and **3**$_{Se}$. Moreover, slightly greater values are observed for the σ-holes opposite the COOH moiety due to its proximity causing a stronger inductive effect. Also, the electron-withdrawing nature of COOH enhances the donor abilities of the chalcogens compared to those in the unsubstituted 2,1,3-benzothiadiazole or 2,1,3-benzoselenadiazole, for which the calculated ESP of the σ-holes is equal to 19.7 and 28.6 kcal/mol, respectively (see Figure S2 in ESI). It is worth noting that in each instance the carboxyl group remains in the plane of the heterocycle, so the whole molecule is flat. This information suggests that there is a great likelihood for molecules to form flat sheets in a crystal lattice stabilised by face-to-face type stacking interactions.

ESP maps are the first indication that hydrogen bonds will be the driving force for the assembly of thiadiazoles, whereas chalcogen bonds, if formed, should have relatively low energy. The situation is different with selenadiazoles. The maximum ESP value of either of the two σ-holes of the Se atom is closer to the value for the

carboxylic H, which suggests that hydrogen and chalcogen bonds are more likely to occur together in the crystal lattice of these compounds.

Based on these facts, four synthons **A**–**D** in the crystal structures of the studied chalcogenadiazolecarboxylic acids are expected (Fig. 6). Since the molecules are carboxylic acids, the acid–acid homosynthon (**A**) can appear in the crystal. It is worth mentioning that this motif is very common for simple aliphatic and aromatic carboxylic acids, but the probability of its formation decreases to 33% in the presence of competing H-bonding functional groups.[64] The second motif that can appear is the four-membered cyclic $[Ch\cdots N]_2$ synthon (**B**). Its formation depends strictly on the chalcogen atom and it occurs much more often in the case of selenium derivatives. Finally, two acid–heterocycle heterosynthons can appear in the crystal lattice, containing either only HB (**C**) or an HB and a ChB (**D**).

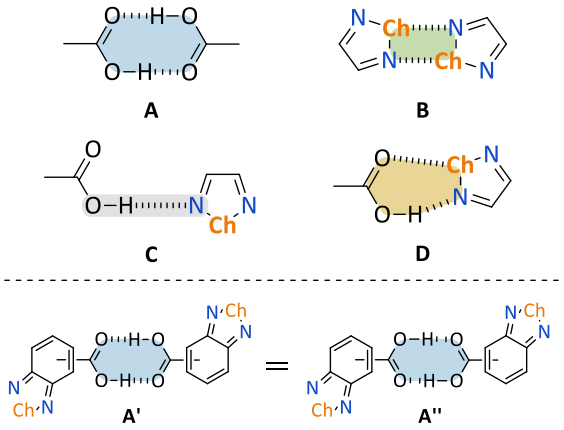

Fig. 6 Supramolecular synthons expected in the crystal lattices of the studied compounds (Ch = S, Se) (top). Supramolecular equivalence of the two variants of synthon **A** (bottom).

The studied molecules, due to the presence of a carboxyl group, are not entirely rigid and can exist as two conformers, which should increase the number of possible motifs in the solid state. However, the two spatial orientations of the acid–acid homosynthon are supramolecularly equivalent (see **A'** and **A''** in Fig. 6). The only factor to be considered is the difference in the interaction energy due to the proximity of other electronegative atoms or functional groups to the synthons. Due to the fact that the *anti* conformations have lower energy (see the Experimental section), it was those conformations that were selected to generate ESP maps.

Crystal structure descriptions

To test the theoretical assumptions presented above, we synthesized the chalcogenadiazolecarboxylic acids and determined their crystal structures, which are described below. Unfortunately, as already mentioned, 1,2,5-selenadiazole-3-carboxylic acid (**1Se**) could not be obtained and therefore its crystal structure is not included.

Compound **1S** crystallises in the triclinic $P\bar{1}$ space group with two independent molecules in the asymmetric unit. The molecules remain in their flat conformation and are connected through O–H···N HBs and S···O ChBs (synthon **D**) into polar chains spreading along the $[\bar{1}01]$ direction and interacting laterally with each other *via* additional hydrogen (C_{Ar}–H···N) and chalcogen (S···O) bonds (Fig. 7). The parameters of HBs and ChBs are presented in Table 1. The chains aggregate into flat sheets parallel to the $(1\bar{1}1)$ plane with the interplanar distance of 3.15 Å, which indicates $\pi\cdots\pi$ interactions. Interestingly, neither homosynthon **A** nor **B** is observed. Instead, a centrosymmetric $[S\cdots O]_2$ motif is present (see Fig. 7), whose analogue $[Ch\cdots X^-]_2$ is characteristic for *N*-alkyl-2,1,3-benzochalcogenadiazolium salts.[65,66]

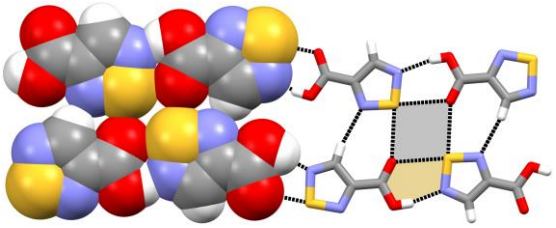

Fig. 7 Intermolecular interactions in the crystal structure of $\mathbf{1_S}$. Selected molecules are represented in spacefill style; heterosynthon **D** is highlighted in yellow, and the $[S\cdots O]_2$ motif – in grey.

Table 1 Parameters of the selected hydrogen and chalcogen bonds in studied the crystals. (i) –1 + *x*, *y*, 1 – *z*; (ii) 2 – *x*, 1 – *y*, 1 – *z*; (iii) 1 – *x*, – *y*, 1 – *z*; (iv) 1 + *x*, *y*, –1 + *z*; (v) 1 – *x*, – *y*, 1 + *z*; (vi) *x*, 1.5 – *y*, 0.5 + *z*; (vii) 1 – *x*, 2 – *y*, 1 – *z*; (viii) 1 – *x*, 1 – *y*, 2 – *z*; (ix) – *x*, 1 – *y*, – *z*; (x) – *x*, 2 – *y*, 1 – *z*; (xi) 1.5 – *x*, 0.5 + *y*, 0.5 – *z*; (xii) 1.5 – *x*, –0.5 + *y*, 0.5 – *z*.

	Y–A···Z	A···Z (Å)	Y···Z (Å)	Y–A···Z (°)
$\mathbf{1_S}$	O1A–H1A···N1B	1.95	2.779 (2)	167
	O1B–H1B···N1A^{i}	1.95	2.774 (3)	167
	N1A–S2A···O2B^{ii}	2.974 (2)	–	173.08 (8)
	N3A–S2A···O2B	2.915 (2)	–	176.24 (8)
	N1B–S2B···O2A^{iii}	2.957 (2)	–	178.09 (8)
	N3B–S2B···O2A^{iv}	2.903 (2)	–	176.04 (8)
$\mathbf{2_S}$	O1–H1···O2^{v}	1.78	2.619 (2)	176
$\mathbf{2_{Se}}$	O1–H1···N1^{vi}	1.92	2.757 (4)	173
	N1–Se2···N3^{vii}	2.864 (4)	–	168.5 (1)
$\mathbf{3_S}$	O1–H1···O2^{viii}	1.59	2.617 (2)	175
	N1–S2···N3^{ix}	3.079 (2)	–	165.8 (8)
$\mathbf{3_{Se}}$	O1–H1···O2^{x}	1.67	2.617 (5)	161
	N1–Se2···N1^{xi}	3.175(3)	–	161.6 (1)
	N3–Se2···N3^{xii}	2.756(3)	–	173.9 (1)

The crystals of $\mathbf{2_S}$ belong to the monoclinic crystal system (space group $P2_1/n$). The carboxyl group of the $\mathbf{2_S}$ molecule again lies within the plane of the heterocycle, which is in accordance with the calculations, but the *syn* conformation is observed. Nonetheless, molecules connect *via* the acid–acid synthon **A** and do not form ChBs (Fig. 8a, Table 1). This leads to the formation of dimers, which are then arranged into tapes assisted with multiple weaker C_{Ar}–H···O and C_{Ar}–H···N HBs (Fig. 8a). Adjacent tapes are twisted by approximately 60° and spread along the [110] and [$\bar{1}$10] directions, and therefore they do not form a layered structure (Fig. 8b). π-Stacking interactions cause the formation of slightly slipped stacks with the interplanar distance of 3.22 Å.

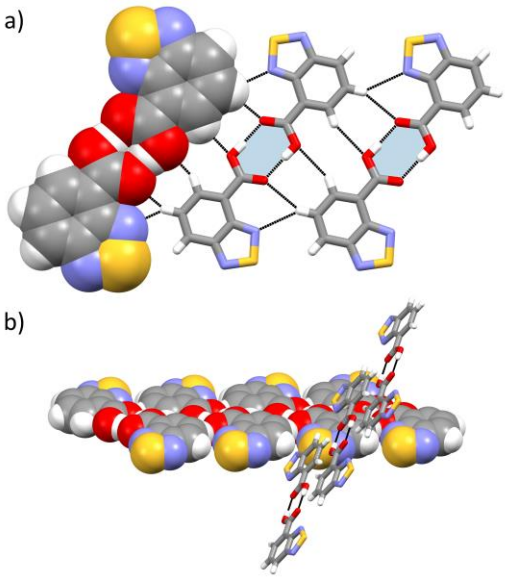

Fig. 8 Crystal structure of $\mathbf{2_S}$: a) fragment of the molecular tape (one dimer is represented in spacefill style and the centrosymmetric carboxylic acid synthon **A** is highlighted in blue); b) mutual orientation of two adjacent tapes of molecules in the crystal structure. Hydrogen bonds are represented by black dotted lines.

The selenium analogue $\mathbf{2_{Se}}$ also belongs to the monoclinic crystal system (space group $P2_1/c$). This time however, the presence of Se atoms favours the formation of ChBs. Interestingly, both synthons **B** and **C** are present (Fig. 9a). Although the molecules aggregate through O–H···N and Se···N bonds (Table 1) and are flat themselves, they cannot form flat tapes due to the steric hindrance between the carbonyl O atom and the benzene ring of the heterocycle (Fig. 9a) – every other molecule is twisted by *ca*. 52°. The polymeric structures are stacked on top of each other and connected not only by π-electron interactions, but also by $[Se\cdots N]_2$ synthons (Fig. 9b). The 3D crystal structure is stabilised by additional interactions. For example, due to the proximity of the two molecules forming the $[Se\cdots N]_2$ synthon, Se···O–H contacts are observed. In addition, each carbonyl oxygen atom is involved in the formation of two C_{Ar}–H···O=C HBs with two neighbouring molecules.

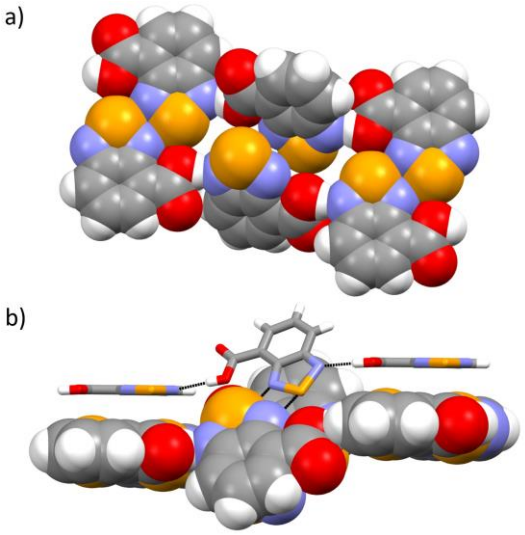

Fig. 9 Crystal structure of $\mathbf{2_{Se}}$: a) fragment of the polymeric structure; b) side view of two fragments connected by synthon **B**. Hydrogen and chalcogen bonds are indicated by black dotted lines.

The crystal structures of isomeric compounds $\mathbf{3_S}$ and $\mathbf{3_{Se}}$ are similar to each other. In both cases, the molecules adopt *anti* conformation (with the carbonyl oxygen atom farther from the heterocyclic nitrogen atom), and both compounds have a layered crystal structure. The main building block in both structures is the dimer of molecules

connected *via* the centrosymmetric carboxylic synthon **A**. The molecules of the sulphur derivative aggregate through chalcogen bonds (centrosymmetric synthon **B**) and form supramolecular tapes (Fig. 10a). The polymeric structures are arranged into layers parallel to $(20\bar{1})$ and held together by C_{Ar}–H···O HBs. Despite the right orientation of the polymers and their proximity to each other, no additional S···N contacts between the adjacent strands are observed – only one of the two S atom σ-holes is used to form the interaction. The 3D structure is stabilized by *π*-stacking interactions and the interplanar distances are equal to 3.01 Å and 3.18 Å.
Similar polymeric structures are observed in the crystal lattice of the selenium derivative **3$_{Se}$**. The molecules form centrosymmetric dimers *via* synthon **A**, and these subunits are connected by the $[Se\cdots N]_2$ synthon (synthon **B**) forming supramolecular tapes (Fig. 10b). The polymeric chains are arranged into layers parallel to (103) and held together by C_{Ar}–H···O HBs and, more importantly, by additional strong Se···N ChBs. In this crystal, both Se atom σ-holes are engaged in the formation of $[Se\cdots N]_2$ synthons. As in **3$_S$**, the layers of the molecules of the selenium derivative are inverted over symmetry centres and the interplanar distances are 3.17 Å and 3.18 Å.

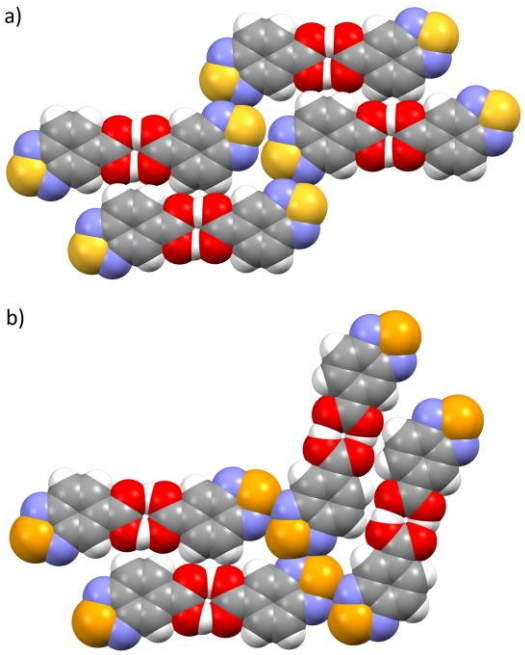

Fig. 10 Crystal structures of **3$_S$** and **3$_{Se}$**: a) fragment of the layer of **3$_S$** molecules; b) fragment of the layer of **3$_{Se}$** molecules.

In the obtained crystals structures homosynthons are the most common. Acid–acid synthons **A** are present in three out of the five crystal structures – the exceptions are **1$_S$** (only synthons **D**) and **2$_{Se}$** (synthons **B** and **C**). $[Ch\cdots N]_2$ synthons are also present in three out of the five crystal lattices – the motif did not form in **1$_S$** and **2$_S$**, for which the strongest interactions are HBs, not ChBs. It is worth emphasizing that there are no intramolecular HBs (**E**, Fig. 11) in any of the obtained crystal structures. Interestingly, synthon **D**, described for cocrystals of benzochalcogenadiazoles with carboxylic acids,[34] was observed only for **1$_S$**.

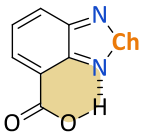

E

Fig. 11 Supramolecular synthon **E** not observed in the crystal lattices of the studied compounds (Ch = S, Se).

During the synthesis of the 2,1,3-chalcogenadiazolecarboxylic acids, we obtained good quality crystals of the acids' methyl esters. Our inspection of the Cambridge Structural Database (CSD v. 5.42, updates Feb. 2024) revealed the structures of ethyl, propyl, isopropyl and butyl 2,1,3-benzochalcogenadiazole-5-carboxylates, but

no methyl esters have been deposited to date. That prompted us to also determine the crystal structures of the obtained esters.

The introduction of a methyl group in the molecule eliminated the possibility of forming carboxylic synthon **A**. Molecules of **4**–**5** no longer possess a strong HB donor, thus their crystal structure is governed mainly by chalcogen and π-stacking interactions. In every instance, $[Ch\cdots N]_2$ synthon (synthon **B**) is present, which for thiadiazoles is still a relatively rare occurrence. In $\mathbf{5_{Se}}$, molecules are arranged into a polymeric structure stabilised by these synthons. Moreover, the proximity of molecules in $\mathbf{4_{Se}}$ causes Se···O contacts to appear (as also observed in $\mathbf{2_{Se}}$). In each structure, $\pi\cdots\pi$ interactions and additional weak C–H···N and/or C–H···O interactions are also present. Figures S3–S5 depicting the crystal structures are presented in ESI.

Intermolecular interaction energies

To compare the obtained crystal structures with theoretical intermolecular interaction energies, we performed calculations of the energies between the studied molecules arranged into the predicted and observed synthons **A**, **B** and **D**. The optimisation process of the molecules forming synthon **C** converged to a structure containing synthon **D**, and as the result these calculations are not included. The interaction energy (ΔE_{int}) was calculated as the difference between the energy of the optimized dimer (E_{dimer}) and the combined energy of two optimized individual molecules of chalcogenadiazolecarboxylic acid ($E_{monomer}$) according to the equation: $\Delta E_{int} = E_{dimer} - 2E_{monomer}$.[67] The results are presented in Table 2.

Table 2 The calculated intermolecular interaction energies ΔE_{int} (in kcal/mol) within synthons **A**, **B** and **D** formed by the studied compounds. The B3LYP/6-31++G** and B3LYP/6-31G** level of theory was used for the sulphur and selenium derivatives respectively. Only centrosymmetric versions of synthons **A** and **B** are presented. Synthon **B** involves only the σ-hole with the highest ESP value.

Compound	synthon		
	A	**B**	**D**
$\mathbf{1_S}$	–14.9	–1.9	–7.6
$\mathbf{1_{Se}}$	–15.4	–4.2	–9.6
$\mathbf{2_S}$	–15.2	–1.4	–7.2
$\mathbf{2_{Se}}$	–15.5	–3.2	–9.1
$\mathbf{3_S}$	–15.9	–1.5	–7.6
$\mathbf{3_{Se}}$	–16.3	–3.6	–9.7

In each instance, the lowest value of the interaction energy was obtained for the acid–acid homosynthon **A** (about –15 kcal/mol). Slightly lower in energy are interactions within synthon **D**, which consists of both a hydrogen and a chalcogen bond. The values reach –8 kcal/mol for thiadiazoles and –10 kcal/mol for selenadiazoles. Lower values for the latter compounds are due to the fact that Se atoms form stronger ChBs (Se···O interactions are stronger than S···O interactions). The calculations showed that synthons **B** comprising two ChBs have the least stabilising effect. The values for $[S\cdots N]_2$ motifs do not exceed –2 kcal/mol, and for selenadiazoles they are about twice as low, which again is attributed to the higher polarizability of the Se atom. Although synthon **A** turned out to be the most stabilizing, it does not appear in the crystal structures of $\mathbf{1_S}$ and $\mathbf{2_{Se}}$. Secondly, despite the large energy difference between synthons **A** and **B**, they appear equally frequently in the crystal structures obtained. The obtained results are not in full agreement with the observations made on the basis of the crystal structures. Nevertheless, energy calculations within synthons alone can indeed be the starting point in predicting crystal structure. The discrepancies may be the result from the fact that calculations usually include one or two types of interaction at a time, while in a crystal, the intermolecular interactions are more complex. For example, π-stacking interactions have a significant impact on the self-organization of molecules in the solid state, but they are often neglected during the structure prediction.

Crystal lattice energies

Lattice energy is a useful indicator of crystal stability and solubility which both come directly from intermolecular interactions within the crystal. The lower (the more negative) the value, the more stable and usually less soluble the crystal of a given compound, due to the greater amount of energy needed to break the interactions, although the dissociation process also releases some energy.[68]

During the characterisation of the final chalcogenadiazolecarboxylic acids we observed that **3_{Se}** clearly differs in its physical properties from the other compounds. It has a much higher melting point (286–287°C), which is relatively rare for an organic compound with such a low molecular weight, and additionally it has markedly reduced solubility in common organic solvents. This is most likely the result of the polymeric crystal structure stabilised by strong intermolecular interactions – both hydrogen and chalcogen bonds – the cooperation of which, together with π-stacking interactions, leads to obtaining quite a stable, layered network of molecules.

This prompted us to also calculate lattice energies of all the acids and investigate the interactions that contribute to the energy of a crystal lattice. We additionally checked whether the higher melting points of the compounds correspond to higher values of the calculated lattice energy. The results are presented in Table 3.

Table 3 Calculated theoretical lattice energies (E_L) and melting points of compounds **1**–**3**. Contributions to the lattice energies: E_c (cohesive energy calculated from the difference in electronic and nuclear repulsion energy of the bulk crystal and the molecules in the bulk), E(D*) (dispersive contribution derived from modified Grimme model) E_{BSSE} (basis set superposition error energy correction). The energies are expressed in kcal·mol^{-1}.

Compound	E_c	E(D*)	$E_L = E_c + E(D^*) + E_{BSSE}$	mp
1_S	–26.2	–3.0	–21.6	162–164°C
2_S	–28.8	–4.5	–24.4	185–189°C
2_{Se}	–32.0	–4.6	–27.4	213–214°C
3_S	–37.2	–4.4	–32.1	220–222°C
3_{Se}	–37.6	–4.6	–31.9	286–287°C

The obtained values correlate quite well with the experimentally measured melting points, i.e. the lower the lattice energy, the higher the melting point of a compound. The lattice energy of **1_S** is the least negative due to the smallest molecule size and relatively weak intermolecular interactions. Moving on to molecules containing an additional benzene ring (**2**–**3**), the lattice energy is lower and reaches the minimum value for **3_S** and **3_{Se}**. The calculations indicate a substantial contribution of the cohesive component E_c to the total lattice energies over the dispersive term E(D*) for all of the studied compounds. This suggests that hydrogen and chalcogen bonds, included mainly in E_c, contribute the most to the energy of the entire crystal lattice. π-Stacking interactions do exist and are the E(D*) constituent, but they are not nearly as stabilising as HBs and ChBs.

The calculations clearly showed that when the COOH is in the 5-position, the melting point is higher due to strong intermolecular interactions and polymeric crystal structure (an analogy to *o*-nitrophenol and *p*-nitrophenol or salicylic acid and *p*-hydroxybenzoic acid where the *para* derivatives have higher melting points due to polymeric crystal structures unlike the *ortho* derivatives for which the strongest hydrogen bonds are formed intramolecularly).[69–72] Also, because of stronger chalcogen bonds, the crystal lattice energies are more negative and the melting points are higher for selenium derivatives. These trends are illustrated in Fig. 12.

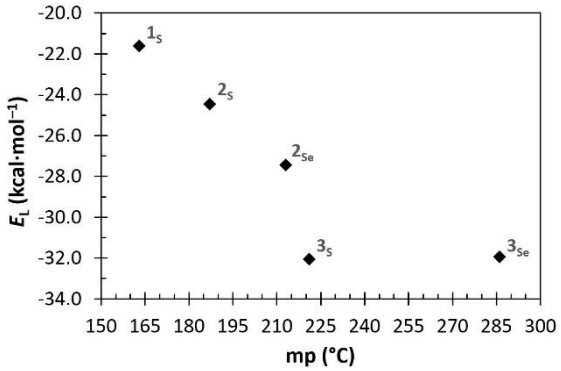

Fig. 12 Relationship between the calculated theoretical lattice energies (E_L) and the melting points of the studied compounds.

Moreover, the calculated lattice energy values for **3$_S$** and **3$_{Se}$** are almost identical, which is due to their very similar crystal structures. The difference in the melting points must therefore result from the strength of the chalcogen interaction – smaller for S, greater for Se.

Conclusions

In summary, the use of derivatives **1**–**3** (bearing both carboxylic and chalcogenadiazole moieties) as simple model compounds, differing in the size of the aromatic unit and the chalcogen atom, allowed us to identify their synthon preferences in the solid state. The results showed that $R_2^2(8)$ self-complementary acid dimers **A** and four-membered $[Ch\cdots N]_2$ rings **B** occur equally frequently and were identified in four of the structures examined. Intermolecular heterosynthons, where the carboxyl group interacts with the chalcogenadiazole moiety *via* one-point (C=O)O–H···N (synthon **C**) or two-point O–H···N–S···O=C interactions (synthon **D**) are less common.
Furthermore, the synthon preference depends on the proximity of the hydrogen and chalcogen bond donors – when they are farther apart, both homosynthons (**A** and **B**) are observed regardless of the chalcogen atom present (**3$_S$** and **3$_{Se}$**). The direct connection of the carboxyl group to the chalcogenadiazole ring (as in **1$_S$**) results in the formation of a network where motif **D** is prevalent.
Moreover, the position of the carboxyl group in **2**–**3** influences their crystal architecture. The location of the COOH in the 5-position in compounds **3$_S$** and **3$_{Se}$** facilitates the formation of a layered structure. In contrast, derivatives **2$_S$** and **2$_{Se}$**, where the carboxyl group is situated in the 4-position, form supramolecular tapes in the solid state. Also, the position of the COOH moiety has a significant impact on the macroscopic properties of the obtained materials. Compound **3$_{Se}$** has a much higher melting point and very poor solubility in common solvents.
The calculated lattice energies of derivatives **1**–**3** indicate that in each case HBs and ChBs interactions make the main contribution to the crystal packing, whereas other interactions account for no more than 20% of the total lattice energy. Also, the value of the crystal lattice energy is the most negative for compounds whose crystal structure is stabilised by both HBs and ChBs.
To sum up, cooperation between hydrogen and chalcogen bonds was observed in the crystal structures obtained and the presence of strong ChB donor does not hinder the formation of hydrogen bonds.

Author contributions

J. Alfuth: conceptualization, investigation, visualization, writing – original draft. A. Czapik: investigations (determination of the crystal structures). B. Zadykowicz: formal analysis (quantum-chemical calculations). T. Olszewska: conceptualization, writing – review.

Conflicts of interest

There are no conflicts to declare.

Acknowledgements

Computations were carried out using the computers of Centre of Informatics Tricity Academic Supercomputer & Network and the Wroclaw Centre for Networking and Supercomputing (WCSS) (Grant No. 215).

References

1 G. R. Desiraju, *Crystal engineering. The design of organic solids*, Elsevier, Amsterdam, 1989.
2 L. C. Gilday, S. W. Robinson, T. A. Barendt, M. J. Langton, B. R. Mullaney and P. D. Beer, *Chem. Rev.*, 2015, **115**, 7118–7195.
3 G. Cavallo, P. Metrangolo, R. Milani, T. Pilati, A. Priimagi, G. Resnati and G. Terraneo, *Chem. Rev.*, 2016, **116**, 2478–2601.

4 K. T. Mahmudov, M. N. Kopylovich, M. F. C. Guedes Da Silva and A. J. L. Pombeiro, *Dalton Trans.*, 2017, **46**, 10121–10138.
5 L. Vogel, P. Wonner and S. M. Huber, *Angew. Chem. Int. Ed.*, 2019, **58**, 1880–1891.
6 A. Daolio, A. Pizzi, G. Terraneo, A. Frontera and G. Resnati, *ChemPhysChem*, 2021, **22**, 2281–2285.
7 A. Daolio, A. Pizzi, M. Calabrese, G. Terraneo, S. Bordignon, A. Frontera and G. Resnati, *Angew. Chem. Int. Ed.*, 2021, **60**, 20723–20727.
8 D. González-Rodríguez and A. P. H. J. Schenning, *Chem. Mater.*, 2011, **23**, 310–325.
9 K. M. Hutchins, *R. Soc. Open Sci.*, 2018, **5**, 180564.
10 N. Biot and D. Bonifazi, *Chem. – A Eur. J.*, 2020, **26**, 2904–2913.
11 A. Haque, K. M. Alenezi, M. S. Khan, W. Wong and P. R. Raithby, *Chem. Soc. Rev.*, 2023, **52**, 454–472.
12 C. B. Aakeröy, S. Panikkattu, P. D. Chopade and J. Desper, *CrystEngComm*, 2013, **15**, 3125–3136.
13 J. C. Gamekkanda, A. S. Sinha, J. Desper, M. Daković and C. B. Aakeröy, *New J. Chem.*, 2018, **42**, 10539–10547.
14 C. C. Robertson, J. S. Wright, E. J. Carrington, R. N. Perutz, C. A. Hunter and L. Brammer, *Chem. Sci.*, 2017, **8**, 5392–5398.
15 C. B. Aakeröy, M. Fasulo, N. Schultheiss, J. Desper and C. Moore, *J. Am. Chem. Soc.*, 2007, **129**, 13772–13773.
16 X. An, H. Zhuo, Y. Wang and Q. Li, *J. Mol. Model.*, 2013, **19**, 4529–4535.
17 F. F. Awwadi, D. Taher, S. F. Haddad and M. M. Turnbull, *Cryst. Growth Des.*, 2014, **14**, 1961–1971.
18 Y. Geboes, F. De Proft and W. A. Herrebout, *Acta Crystallogr. Sect. B*, 2017, **73**, 168–178.
19 J. Lombard, T. Le Roex and D. A. Haynes, *Cryst. Growth Des.*, 2020, **20**, 7384–7391.
20 E. Jaime-Adán, S. Hernández-Ortega, R. A. Toscano, J. M. Germán-Acacio, A. D. Sánchez-Pacheco, M. Hernández-Vergara, J. E. Barquera and J. Valdés-Martínez, *Cryst. Growth Des.*, 2024, **24**, 1888–1897.
21 V. De Silva, P. Le Magueres, B. B. Averkiev and C. B. Aakeröy, *Acta Crystallogr. Sect. C*, 2022, **78**, 716–721.
22 M. D. Esrafili, S. Asadollahi and Y. Dadban Shahamat, *Struct. Chem.*, 2016, **27**, 1439–1447.
23 Y. Ishigaki, K. Shimomura, K. Asai, T. Shimajiri, T. Akutagawa, T. Fukushima and T. Suzuki, *Bull. Chem. Soc. Jpn.*, 2022, **95**, 522–531.
24 J. Alfuth, B. Zadykowicz, B. Wicher, K. Kazimierczuk, T. Połoński and T. Olszewska, *Cryst. Growth Des.*, 2022, **22**, 1299–1311.
25 V. De Silva, B. B. Averkiev, A. S. Sinha and C. B. Aakeröy, *Molecules*, 2021, **26**, 4125.
26 Y. Zhang, B. Ji, A. Tian and W. Wang, *J. Chem. Phys.*, 2012, **136**, 141101.
27 X. Guo, Y. W. Liu, Q. Z. Li, W. Z. Li and J. B. Cheng, *Chem. Phys. Lett.*, 2015, **620**, 7–12.
28 P. Sanz, M. Yáñez and O. Mó, *J. Phys. Chem. A*, 2002, **106**, 4661–4668.
29 G. Sánchez–Sanz, I. Alkorta and J. Elguero, *Molecules*, 2017, **22**, 227.
30 S. Scheiner, *Phys. Chem. Chem. Phys.*, 2022, **24**, 28944–28955.
31 S. Miao, Y. Zhang, L. Shan, M. Xu, J.-G. Wang, Y. Zhang and W. Wang, *Crystals*, 2021, **11**, 1309.
32 S. Langis-Barsetti, T. Maris and J. D. Wuest, *J. Org. Chem.*, 2017, **82**, 5034–5045.
33 L. J. Riwar, N. Trapp, K. Root, R. Zenobi and F. Diederich, *Angew. Chem. Int. Ed.*, 2018, **57**, 17259–17264.
34 K. Eichstaedt, A. Wasilewska, B. Wicher, M. Gdaniec and T. Połoński, *Cryst. Growth Des.*, 2016, **16**, 1282–1293.
35 Y.-L. Xiao, B. Zhang, C.-Y. He and X. Zhang, *Chem. Eur. J.*, 2014, **20**, 4532–4536.
36 J. E. Barnsley, G. E. Shillito, C. B. Larsen, H. van der Salm, L. E. Wang, N. T. Lucas and K. C. Gordon, *J. Phys. Chem. A*, 2016, **120**, 1853–1866.
37 I. Idris, T. Tannoux, F. Derridj, V. Dorcet, J. Boixel, V. Guerchais, J. F. Soulé and H. Doucet, *J. Mater. Chem. C*, 2018, **6**, 1731–1737.
38 S. Hayashi, T. Koizumi and N. Kamiya, *Cryst. Growth Des.*, 2017, **17**, 6158–6162.
39 M. S. Taylor, *Coord. Chem. Rev.*, 2020, **413**, 213270.
40 S. Shi, Q. Liao, H. Wang and G. Xiao, *New J. Chem.*, 2020, **44**, 8032–8043.
41 E. Xu, H. Zhong, H. Lai, D. Zeng, J. Zhang, W. Zhu and Q. Fang, *Macromol. Chem. Phys.*, 2010, **211**, 651–656.
42 E. R. T. Tiekink, *Coord. Chem. Rev.*, 2021, **443**, 214031.
43 Rigaku Oxford Diffraction, *CrysAlisPro software system, version 171.41*, Rigaku Corporation, Wrocław, Poland, 2020.
44 G. M. Sheldrick, *Acta Crystallogr. Sect. A* , 2015, **71**, 3–8.
45 G. M. Sheldrick, *Acta Crystallogr. Sect. C*, 2015, **71**, 3–8.
46 C. F. Macrae, I. Sovago, S. J. Cottrell, P. T. A. Galek, P. McCabe, E. Pidcock, M. Platings, G. P. Shields, J. S. Stevens, M. Towler and P. A. Wood, *J. Appl. Crystallogr.*, 2020, **53**, 226–235.

47 A. D. Becke, *J. Chem. Phys.*, 1993, **98**, 1372–1377.
48 A. D. Becke, *J. Chem. Phys.*, 1993, **98**, 5648–5652.
49 C. Lee, W. Yang and R. G. Parr, *Phys. Rev. B*, 1988, **37**, 785–789.
50 P. C. Hariharan and J. A. Pople, *Theor. Chim. Acta*, 1973, **28**, 213–222.
51 W. J. Hehre, L. Radom, P. V. R. Schleyer and J. A. Pople, *Ab Initio Molecular Orbital Theory*, John Wiley & sons Ltd., New York, 1986.
52 M. J. Frisch, G. W. Trucks, H. B. Schlegel, G. E. Scuseria, M. A. Robb, J. R. Cheeseman, G. Scalmani, V. Barone, G. A. Petersson, H. Nakatsuji, X. Li, M. Caricato, A. V. Marenich, J. Bloino, B. G. Janesko, R. Gomperts, B. Mennucci, H. P. Hratchian, J. V. Ortiz, A. F. Izmaylov, J. L. Sonnenberg, D. Williams-Young, F. Ding, F. Lipparini, F. Egidi, J. Goings, B. Peng, A. Petrone, T. Henderson, D. Ranasinghe, V. G. Zakrzewski, J. Gao, N. Rega, G. Zheng, W. Liang, M. Hada, M. Ehara, K. Toyota, R. Fukuda, J. Hasegawa, M. Ishida, T. Nakajima, Y. Honda, O. Kitao, H. Nakai, T. Vreven, K. Throssell, J. A. Montgomery Jr., J. E. Peralta, F. Ogliaro, M. J. Bearpark, J. J. Heyd, E. N. Brothers, K. N. Kudin, V. N. Staroverov, T. A. Keith, R. Kobayashi, J. Normand, K. Raghavachari, A. P. Rendell, J. C. Burant, S. S. Iyengar, J. Tomasi, M. Cossi, J. M. Millam, M. Klene, C. Adamo, R. Cammi, J. W. Ochterski, R. L. Martin, K. Morokuma, O. Farkas, J. B. Foresman and D. J. Fox, *Gaussian 16 (Revision C.01)*, Gaussian, Inc., Wallingford CT, 2019.
53 R. D. Dennington, T. A. Keith and J. M. Millam, *GaussView, version 6.1.1*, Semichem Inc., Shawnee Mission, KS, 2019.
54 M. M. Francl, W. J. Pietro, W. J. Hehre, J. S. Binkley, M. S. Gordon, D. J. DeFrees and J. A. Pople, *J. Chem. Phys.*, 1982, **77**, 3654–3665.
55 G. W. Spitznagel, T. Clark, P. von Ragué Schleyer and W. J. Hehre, *J. Comput. Chem.*, 1987, **8**, 1109–1116.
56 S. F. Boys and F. Bernardi, *Mol. Phys.*, 1970, **19**, 553–566.
57 R. Dovesi, A. Erba, R. Orlando, C. M. Zicovich-Wilson, B. Civalleri, L. Maschio, M. Rérat, S. Casassa, J. Baima, S. Salustro and B. Kirtman, *WIREs Comput. Mol. Sci.*, 2018, **8**, e1360.
58 J. K. Labanowski and J. K. Andzelm, *Density functional methods in chemistry*, Springer, New York, 1991.
59 Y. Zhao and D. G. Truhlar, *Theor. Chem. Acc.*, 2008, **120**, 215–241.
60 S. Grimme, *J. Comput. Chem.*, 2004, **25**, 1463–1473.
61 S. Grimme, *J. Comput. Chem.*, 2006, **27**, 1787–1799.
62 B. Civalleri, C. M. Zicovich-Wilson, L. Valenzano and P. Ugliengo, *CrystEngComm*, 2008, **10**, 405–410.
63 B. Sandhu, A. McLean, A. S. Sinha, J. Desper and C. B. Aakeröy, *Chemistry*, 2021, **3**, 612–629.
64 F. H. Allen, W. D. Samuel Motherwell, P. R. Raithby, G. P. Shields and R. Taylor, *New J. Chem.*, 1999, **23**, 25–34.
65 L. M. Lee, V. B. Corless, M. Tran, H. Jenkins, J. F. Britten and I. Vargas-Baca, *Dalton Trans.*, 2016, **45**, 3285–3293.
66 J. Alfuth, B. Zadykowicz, A. Sikorski, T. Połoński, K. Eichstaedt and T. Olszewska, *Materials*, 2020, **13**, 4908.
67 J. Hernández-Trujillo, F. Colmenares, G. Cuevas and M. Costas, *Chem. Phys. Lett.*, 1997, **265**, 503–507.
68 J. J. Du, S. A. Stanton, S. Fakih, B. A. Hawkins, P. A. Williams, P. W. Groundwater, J. Overgaard, J. A. Platts and D. E. Hibbs, *Cryst. Growth Des.*, 2021, **21**, 4259–4275.
69 C. D. Sessler, M. Rahm, S. Becker, J. M. Goldberg, F. Wang and S. J. Lippard, *J. Am. Chem. Soc.*, 2017, **139**, 9325–9332.
70 G. Wójcik and I. Mossakowska, *Acta Crystallogr. Sect. B* , 2006, **62**, 143–152.
71 R. Montis and M. B. Hursthouse, *CrystEngComm*, 2012, **14**, 5242–5254.
72 J. J. Du, S. A. Stanton, P. A. Williams, J. A. Ong, P. W. Groundwater, J. Overgaard, J. A. Platts and D. E. Hibbs, *Cryst. Growth Des.*, 2018, **18**, 1786–1798.